Applied Catalysis A, General 629 (2022) 118426

Contents lists available at ScienceDirect

Applied Catalysis A, General

journal homepage: www.elsevier.com/locate/apcata

The physicochemical and catalytic properties of clay extrudates in cyclization of citronellal

Zuzana Vajglová [a], Irina L. Simakova [b], Kari Eränen [a], Päivi Mäki-Arvela [a], Narendra Kumar [a], Markus Peurla [c], Stiina Tolvanen [a], Alexander Efimov [d], Leena Hupa [a], Jouko Peltonen [a], Dmitry Yu. Murzin [a,*]

[a] Åbo Akademi University, Johan Gadolin Process Chemistry Centre, Henriksgatan 2, Turku/Åbo 20500, Finland
[b] Boreskov Institute of Catalysis, Novosibirsk 630090, Russia
[c] Institute of Biomedicine, University of Turku, Kiinamyllynkatu 10, FI-20520 Turku, Finland
[d] Tampere University, Korkeakoulunkatu 8, 33720 Tampere, Finland

ARTICLE INFO

Keywords:
Clay
Extrudates
Citronellal cyclization
Bentonite
Attapulgite
Sepiolite
Palygorskite

ABSTRACT

Four clay materials, namely, bentonite, bleaching earth, attapulgite and sepiolite, were shaped into the cylindrical body by extrusion. Clays were characterized in depth by TEM, SEM-EDX, N_2 physisorption, pyridine FTIR, pH measurements, contact angle measurements, ^{27}Al MAS NMR, and the crush test. Catalytic properties were investigated in the citronellal cyclization as a model reaction. The reaction was performed in the trickle-bed reactor at 70 °C, 10 bar of Ar with 0.086 M initial citronellal concentration in cyclohexane. The best results were obtained over attapulgite with isopulegols yield of 24% and stereoselectivity to the desired isopulegol isomer of 61%. Attapulgite had the highest meso-to-micropore volume ratio, the highest basicity, a low Brønsted-to-Lewis acid sites ratio, and the lowest amount of Brønsted acid sites compared to other extrudates. In addition, same clay exhibited the highest mechanical strength of extrudates.

1. Introduction

Clays are low-cost and simultaneously very important materials comprising clay minerals, which impart their physical properties, such as rheological properties, ion exchange, swelling, hydration, and plasticity [1–9]. Due to these properties, clays have a wide variety of technological and industrial applications [1–3], including their utilization as inorganic binders for scale-up of the catalyst from powder into the shaped bodies used in the industry [10–17]. Larger particles of catalyst avoid an extremely high pressure drop in fixed-bed reactors. Generally, the clay minerals are hydrous aluminium silicates, containing alkaline and alkaline earth elements or even iron [2,4]. Application of clay binders in the shaping process improves stability of the extrudates after shaping and mechanical strength of the final extrudates [13,15]. Coherent networks formed by the particles of clay can deform and restore their shape again when the stress is removed [1,2]. The water molecules adsorb on the clay mineral surfaces by forming a rigid film of a certain order. The presence of water links the clay particles together and determines the nature of plasticity [1,18]. Among the most important industrial clays are kaolin, bentonite, attapulgite (palygorskite), sepiolite, and common clays and shales [1,2].

The use of clays as an inorganic binder in the zeolites pellets or extrudates have been demonstrated in several studies [3,10,11,13–17, 19–21]. The effect of the agglomeration of the ZrO_2/n-ZSM-5 catalysts with bentonite and attapulgite clays was investigated in lignocellulose catalytic pyrolysis [10]. Mordenite and Y zeolite catalysts in the form of pellets containing attapulgite or other clay binders were tested in toluene alkylation with methanol [21]. Montmorillonite clay binder in mesoporous extrudates was investigated in the context of natural gas and biogas purification [16]. Titanium silicalite (TS-1) extrudates with a sepiolite binder were tested in propylene epoxidation with hydrogen peroxide [20]. Formulated clay adsorbents prepared from bentonite were used in small-scale water filter systems [17]. Catalytic pyrolysis of crude glycerol for the synthesis of bio-based benzene, toluene and xylenes (bio-BTX) was performed over ZSM-5 extrudates containing bentonite [19]. The hydroisomerization of n-hexane was performed over Pt/H-Beta-25 extrudates containing bentonite binder [14]. Bentonite and montmorillonite clay binders in Pd/HZSM-5 zeolite catalyst with

* Corresponding author.
E-mail address: dmurzin@abo.fi (D.Yu. Murzin).

https://doi.org/10.1016/j.apcata.2021.118426
Received 26 August 2021; Received in revised form 1 November 2021; Accepted 2 November 2021
Available online 9 November 2021

different Si/Al ratios were studied in the hydroisomerization of n-butane [3]. Bentonite clay binder was also used in Beta and Y extrudates in citronellal cyclization [13,15] and in Ru-, Pt-Beta extrudates in synthesis of menthol from citronellal [11].

Clay materials reported in the literature as an inorganic binder were applied because of their physicochemical properties as well as their low cost. Inorganic binders in the extrudates, in principle, are expected to act as diluents of the active phase, even if clays themselves may have some catalytic properties or inhibitory effects [10,13]. In addition, presence of a binder in extrudates may significantly change the physico-chemical properties of the final material because of, for example, chemical interactions with the active phase [10–15,21–32]. Understanding the role of a clay binder in a particular process may accelerate development of shaped catalysts with superior catalytic performance.

This work is dealing with the catalytic impact of low-cost clay binders on a model reaction in a continuous mode without presence of any additional catalytic material. For this purpose, bentonite, an industrial bleaching earth, attapulgite and sepiolite as the representative of the most common clays applied as inorganic binders in scaling-up of catalysts were selected [3,10–17,19–21]. The clay materials were shaped into cylindrical bodies as extrudates, and tested in the trickle-bed reactor. On the basis of our previous research with zeolite extrudates containing a bentonite binder [13,15] in the citronellal cyclization, an example of the synthesis of fine chemicals promoted by acidic catalysts [11,13,15,22,23,33–43], was the same reaction selected as a model reaction to test the catalytic properties of pure clay binders in the form of extrudates without the presence of any additional acidic catalytic material. Previously the same reaction was considered by the authors as a part of a more complex reaction network for production of menthol from citral using zeolite extrudates shaped with various binders [13,22,23]. To achieve a high selectivity, cyclohexane as a solvent with a low dielectric constant (2.02) and weak interactions with the surface was utilized [22,44,45]. In the current work, the solvent selection as well as the reaction conditions remained the same as previously used for a more complicated reaction network of one –pot citral to menthol transformations, i.e. 70 °C, 10 bar and 0.086 M initial concentration of citronellal in cyclohexane.

2. Experimental

2.1. Preparation of the powder sample and extrudates

Four clay materials were selected, shaped and characterized in the powder form and extrudates, namely: bentonite ($Al_2H_2O_6Si$, VWR International), an industrial bleaching earth (sepiolite [46,47]), attapulgite/palygorskite ($(Mg,Al)_2Si_4O_{10}(OH)\cdot 4H_2O$, Gelest), and sepiolite ($Mg_2H_2SiO_9\cdot xH_2O$, Sigma-Aldrich). All clay materials were sieved into a fraction < 63 μm. The respective suspensions containing a clay material, water and methylcellulose were shaped using a one-screw extrusion device (TBL-2, Tianjin Tianda Beiyang Chemical Co. Ltd., China) into cylindrical-shaped bodies, passing through the holes of 1.5 mm [13,15]. The suspension for extrusion contained 1 wt% of methylcellulose as an organic binder and different amounts of water (37–56 wt%) for each clay material (Table 1). Extrudates were dried in an oven at 100 °C for 7 h. Subsequently, the extrudates were calcined in the muffle oven at 500 °C for 4 h and cut to a length of ca. 10 mm.

Table 1
Weight ratio of the suspension for extrusion with a relative error ±0.2%, and diameter of the final extrudates (d_E).

No.	Sample	Clay *wt%*	Water	MC*	d_E *mm*	sk_r * * *%*	pH* ** -
1	Bentonite	61.8	37.2	1	1.42	5.3	4.4
2	Bleaching earth	54.9	44.1	1	1.38	8.0	4.2
3	Attapulgite	53.1	45.9	1	1.36	9.3	9.9
4	Sepiolite	42.9	56.1	1	1.30	13.3	8.5
5	Bindzil[13]	–	–	–	–	–	9.4

*MC – methylcellulose; **sk_r – relative radial shrinkage, *** pH was measured for 40 mg of the powder binder in 20 mL of distilled water with stirring at 250 rpm.

The diameter of the final extrudates (1.3–1.42 mm) linearly decreased with decreasing concentration of the clay material in the suspension for extrusion (Table 1). The same trend was observed in the literature [48] dealing with extrusion of gadolinia-doped ceria ceramic pastes. The higher solid content in the suspension corresponded to a larger shrinkage following a linear relationship with respect to the solid loading (x in %): the relative radial shrinkage in % is equal to −0.35x+19.0 for ceramic suspensions [48] and −0.43x+31.7 for clay suspensions. A comparison with extrudates containing 70 wt% of the catalyst (H-Beta-25, Ru/H-MCM-41) and 30 wt% of a binder (bentonite, SiO_2: Bindzil, Ludox, Snowtex) [13,15,22,23] shows, that the shrinkage dependence of the solid concentration depends also on the type of material.

For comparison, also a pristine colloidal silica bindzil without impurities (Bindzil-50/80, 50% colloidal SiO_2 in H_2O from Akzo Nobel) was selected and characterized in the current work. Contrary to the expectations, bindzil extrudates could not be shaped alone, even if, bindzil is a very suitable inorganic binder allowing easy shaping of zeolites [13,15,24] and mesoporous catalytic materials [22,23]. Water from the colloidal silica (i.e. bindzil) was evaporated under vacuum at 40 °C and 50 rpm and then the material was dried in an oven overnight. Finally, dry bindzil was sieved into a fraction < 63 μm and characterized.

2.2. Characterization of the powder sample and extrudates

All clay materials were characterized in detail. Morphologies of clays were investigated by transmission (TEM, JEOL JEM-1400Plus) and scanning electron microscopy (SEM, Zeiss Leo Gemini 1530). Determination of the particle sizes was done from TEM and SEM images using the ImageJ program [49]. Energy dispersive X-ray microanalysis (EDX, Zeiss Leo Gemini 1530) was used to determine the composition. Textural properties were studied by nitrogen physisorption (Micrometrics 3Flex-3500). The specific surface area and porosity (pore volume, pore size distribution) were calculated using the Dubinin-Radushkevich (DR) or the Brunauer–Emmett–Teller (BET), and the density functional theory methods, respectively. The amount and strength of Brønsted and Lewis acid sites were determined by Fourier transform infrared spectroscopy using pyridine (≥99.5%) as the probe molecule (with ATI Mattson FTIR Infinity Series spectrometer) using the molar extinction parameters previously reported by Emeis [50]. The thin pellet of catalyst (10–20 mg) was placed in the measurement cell. The catalyst was outgassed under vacuum (0.08 mbar) at 450 °C for 2 h prior to pyridine adsorption, and the background spectra were obtained at 100 °C. Pyridine was adsorbed for 30 min, and then the spectra were collected at 100 °C after heating the sample to 250, 350, and 450 °C, respectively. The Lewis acidity was calculated using the absorption band at 1450 cm^{-1} and the Brønsted acidity using the adsorption band at 1550 cm^{-1}. The temperature, at which pyridine desorbs from the catalyst, was used to classify the acid sites strength. In the calculations of weak, medium, and strong acid sites, the catalyst weight was taken into account. The average peak area (S) was calculated from the six integrated absorbances of Brønsted or Lewis bands at a given temperature. For calculation of the strong acid sites their number as related to those sites corresponding to the peak area measured at 450 °C (i.e. $S_{strong} = S_{450\ °C}$), while for medium and weak acid sites the following equations were respectively used $S_{medium} = S_{350\ °C} - S_{450\ °C}$ and $S_{weak} = S_{250\ °C} - S_{350\ °C}$. The total acidity is considered as the sum of weak, medium and strong acid sites. Measurement of slurry pH were done using pH meter (Mettler Toledo) with 40 mg of the clay powder in 20 mL of distilled water, agitated at 250 rpm. The contact angle was measured using the goniometer CAM 200 (KSV Instruments) for the powder clay with 1 wt% of methylcellulose

pressed into thin pellets. Before measurements, the samples were dried at 100 °C overnight and kept in a desiccator to avoid sorption of moisture from the atmosphere. Water droplets of 2 μL were placed on the surface of each pellet, and the profile of the droplets on the surface was captured by the instrument for 25 frames per drop with a frame interval of 10 frames/ms. A 7–10 amount of drops per sample was analyzed. The mechanical strength of extrudates was tested by crush test (SE 048, Lorentzen & Wettre). For each sample, the average from 10 measurements in vertical and horizontal positions was calculated.

^{27}Al MAS NMR spectra were measured at 130.33 MHz on JEOL JNM-ECZ500R spectrometer equipped with 3.2 mm NM-84007HX expanded VT MAS probe. Spectra were recorded with 0.173 μs (π/12) pulses, 0.2 s delay and 2048 scans for each sample. The *depth2* background suppression was applied to cancel the residual signal of the probe.

Other details of the characterization methods and equipment are presented in our previous publications [12,13,15].

2.3. Catalytic tests

To investigate catalytic properties of clay binder extrudates, the citronellal cyclization was selected as a model reaction. Four different clay extrudates of 0.45 g with the size 10 × 1.3–1.42 mm (Table 1) were mixed with 14.4 g of inert quartz (SiO_2) and loaded into the parallel trickle-bed reactors (ID 12.5 mm, [11,13,15,22,23]). The reaction was performed at 70 °C, 10 bar of Ar, 0.3 mL/min of citronellal in cyclohexane with initial citronellal concentration 0.086 M, 50 mL/min of Ar and the liquid residence time of 5.3 min. The reactants flowed from the top to the bottom.

After dilution with cyclohexane solvent, the liquid samples were analyzed by applying Agilent GC 6890 N equipped with an FID detector and a DB-1 column (length 30 m, internal diameter 250 μm, and film thickness 0.5 μm). The temperature program started at 110 °C followed by a temperature gradient to 130 °C at a ramp 0.4 °C/min and then increasing to 200 °C at a ramp 13 °C/min. The mobile phase was helium. The temperature of the FID detector was 340 °C. The following chemicals were used to calibrate the GC: citronellal, isopulegol, di-methyl octanol, citronellol, nerol, gerneol, and α-terpinene. The other products were confirmed with an Agilent GC/MS 6890 N/5973 N using the same column and the temperature program [11,13,15,22,23].

The liquid residence time (RT) in the trickle-bed reactor was calculated according to the following equation: $RT = V_{CB} \bullet \varepsilon_{CB}/Q_{v(l)}$, where V_{CB} is the catalyst bed volume (4 mL), ε_{CB} is porosity of the catalyst bed (0.4) and $Q_{v(l)}$ is the feedstock volumetric flowrate (0.3 mL/min) [15]. The reaction rate (r) in the trickle-bed reactor was calculated as follows: $r = \Delta\dot{n}/m_{cat}$, where $\Delta\dot{n}$ denotes the change in molar flow rate of the feed at time zero and time t, m_{cat} is catalyst mass [22,23,51].

3. Results and discussion

3.1. Characterization results of the powder sample and extrudates

A pH measurement of clay suspensions revealed acidic values for bentonite and bleaching earth while alkaline values were determined for attapulgite, sepiolite and the reference bindzil (Table 1). The highest

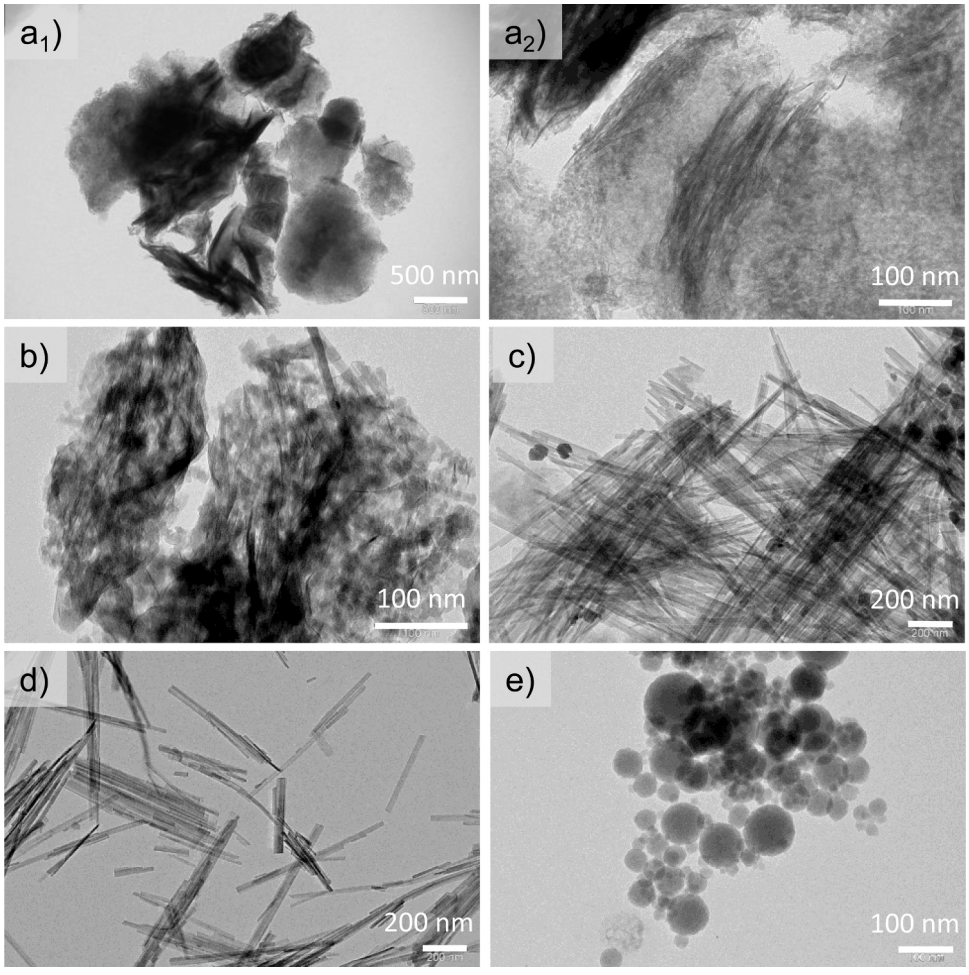

Fig. 1. TEM images of the powder clays: (a) bentonite (scale 500 and 100 nm), (b) bleaching earth (scale 100 nm), (c) attapulgite (scale 200 nm), (d) sepiolite (scale 200 nm), (e) bindzil (scale 100 nm) [13].

value of 9.9 was obtained for attapulgite and the lowest one of 4.2 for an industrial bleaching earth (sepiolite).

TEM (Fig. 1) and SEM (Fig. 2) images clearly show different morphology of the four clay materials. TEM images of bentonite and the bleaching earth (Fig. 1a,b) reveal two phases (small crystals and fibers). The length and width of the fibers determined by TEM for bentonite was 55 and 0.6 nm (Table 2), respectively, which are typical dimensions of montmorillonite [4,12]. A high flexibility of the montmorillonite fibers is attributed to their high aspect ratio (L/W = 92, Table 2). For bleaching earth the length and width of the fibers were determined to be 30 and 0.6 nm (Table 2), respectively, i.e. ca. a half length compared to fibers of bentonite.

On the contrary, attapulgite consisted of a few larger crystals (45 nm) and needle-shaped or rodlike-shaped particles (LxW = 630 × 15 nm) with a lower aspect ratio (L/W = 42) (Fig. 1c, Table 2). Slightly longer and thicker needle-shaped or rodlike-shaped particles (LxW = 650 × 20 nm) were observed for sepiolite without any other phase (Fig. 1d, Table 2). This morphology is attributed to a chain silicate [4,9]. A comparable morphology of sepiolite with a determined diameter of fibrous minerals materials of 60–100 nm was also reported in [52].

Colloidal silica bindzil consists only of round-shaped particles with a broad range of different sizes (4–160 nm, Table 2, [13]).

Table 2
Median, minimum (min), and maximum (max) particle size in nm determined by TEM. Legend: L – length, W – width.

No.	Sample	crystal		fiber/needle-shape			
		median	*min-max*	*LxW*	*L/W*	*min-max (L)*	*min-max (W)*
1	Bentonite	< limit	–	55 × 0.6	92	15–150	0.2–0.8
2	Bleaching earth	< limit	–	30 × 0.6	50	7–100	0.3–1.3
3	Attapulgite	45	25–80	630 × 15	42	115–1200	6–23
4	Sepiolite	–	–	650 × 20	33	110–1260	10–30
5	Bindzil [13]	30	4–160	–	–	–	–

Overall, it can be concluded that the morphology of bentonite is similar to the bleaching earth, and attapulgite is close to sepiolite, which is also in line with SEM images (Fig. 2). On the other hand, fibers of bentonite and bleaching earth were not observed by SEM (Fig. 2a,b). For bentonite, SEM analysis revealed a non-amorphous structure, containing platelets with sharp edges. The particle size of bentonite determined by SEM was 450 nm on median and the largest particles reached ca. 28 μm

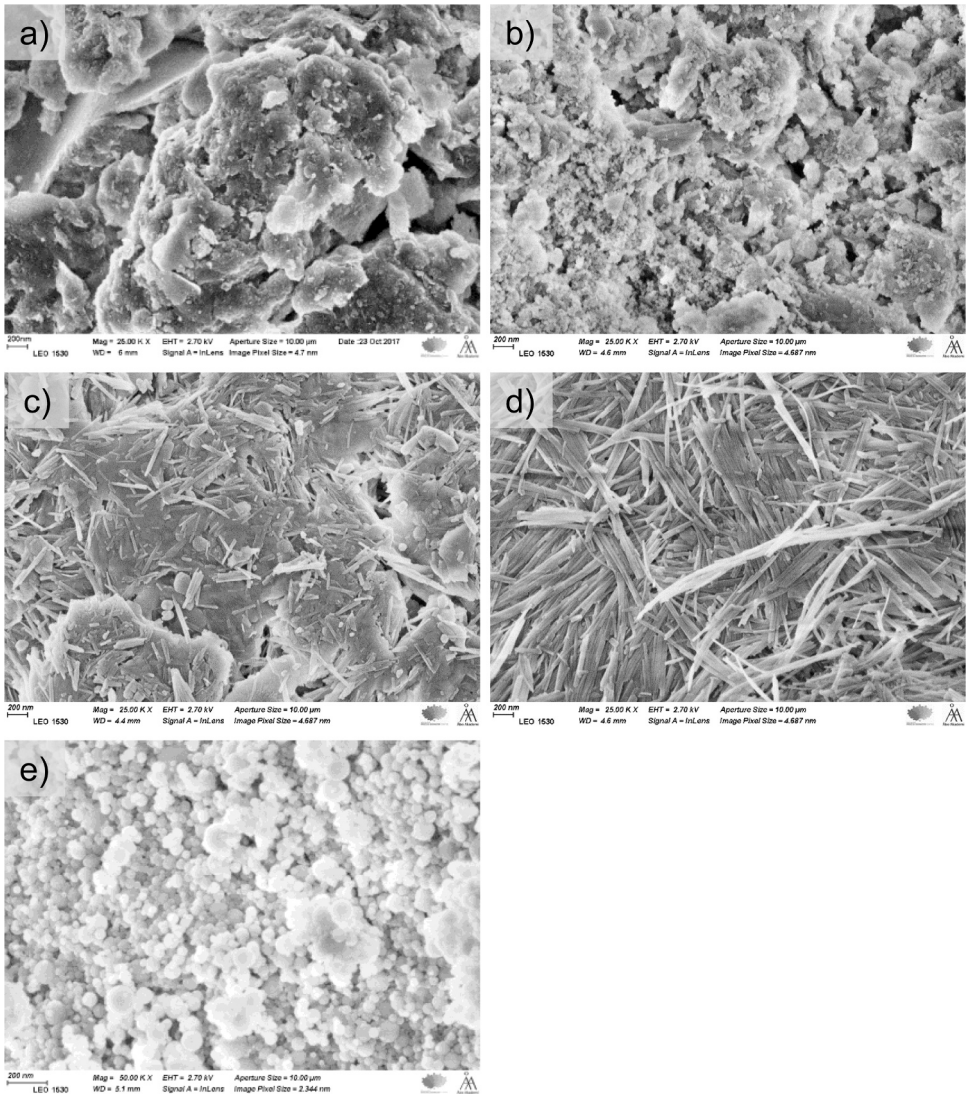

Fig. 2. SEM images of powder clay: (a) bentonite, (b) bleaching earth, (c) attapulgite, (d) sepiolite, (e) bindzil.

[12]. The observed average particle size was attributed to presence of illite comprising 80% of bentonite and less than 5% of kaolinite characterized by the unique large particles [12,53]. The particle size of the bleaching earth determined by SEM was 195 nm on median with the range of the particle sizes being also significantly narrower compared to bentonite (Table 3). In the case of attapulgite, three phases were observed, namely large platelets (1 μm), small round shape particles (110 nm) and needle-shaped or rodlike-shaped particles (LxW = 170 × 20 nm) (Fig. 2c, Table 3). Only one phase, a long needle-shaped or rodlike-shaped particles (LxW = 740 × 30 nm with the maximum length up to 3.1 μm) that occurred as intermeshed, was observed for sepiolite (Fig. 2d, Table 3).

The particle size of round shape bindzil determined by SEM was in the range of 10 – 280 nm.

The elemental analysis revealed different chemical compositions of clay materials (Table 4) which is in line with different morphology observed on TEM and SEM images (Figs. 1 and 2). All samples contained Si (21–29 wt%), Al (1–7 wt%), Mg (1–11 wt%) and K (0.5–1 wt%). Except for sepiolite, 2 wt% of iron was also detected for clay materials. In addition, the bleaching earth and attapulgite contained small amounts (≤ 1 wt%) of other elements, such as Ca, S, Ba, and Ca, P. The least impurities and at the same time the highest Si/Al ratio (16) and the highest Mg content (11 wt%) were observed for sepiolite. On the contrary, the lowest Si/Al ratio (4) and the lowest Mg content (1 wt%) were observed for bentonite. Most impurities were detected in the bleaching earth. The value of the Si/Al ratio higher than the theoretical one is related to the presence of hexagonal SiO_2 (quartz). This is in line with XRD data, which show that bentonite, used in the current work, consisted of peaks originating from illite (80 ± 10 wt%, monoclinic), montmorillonite (< 5 wt%, hexagonal), kaolinite (< 5 wt%, triclinic) and SiO_2 (20 ± 10 wt%, hexagonal) [12]. It should be also noted, that the composition of clays, as well as the morphology, strongly depends on the nature of their genesis. Therefore, the published data for the Si/Al ratio for bentonite vary from 1.7 to 8.2 [19,54–67].

On the contrary, bindzil contained no impurities, only Si (37 wt%), Al (0.2 wt%) and Na (0.6 wt%) were detected (Table 4).

The total acidity of clay materials (Table 5) was as follows: sepiolite (73 μmol/g) > bentonite, bleaching earth (54 μmol/g) > attapulgite (40 μmol/g). No strong acid sites were detected in any sample. This is in line with the expectations as tetrahedral Al atoms are framework substitutions in Si tetrahedral layers. For bentonite and the bleaching earth, the Brønsted-to-Lewis acid sites ratio was 2 and 6, respectively. A high amount of the Brønsted acid sites in clays is in line with low pH values (ca. 4, Table 1). On the contrary, 6-fold and 8-fold more Lewis than Brønsted acid sites were observed for attapulgite and sepiolite, respectively.

A comparison with the literature [68] showed a similar amount of total acid sites of 59 μmol/g for bentonite. On the contrary, ca. three-fold higher value of 145 μmol/g was reported in [69]. This could be related to a slightly higher amount of Fe, Mg, and the presence of others components such as Na, Ca, Mn, P and Ti. However, the detailed acidity data for clay materials are still lacking in the open literature.

On the contrary, bindzil can be considered as a non-acidic material, exhibiting only 2 μmol/g of total acid sites (Table 5, [23]).

All four clay materials contained 13 – 22% of micropores, therefore, in addition to the Brunauer-Emmett-Teller method (BET), the Dubinin-Radushkevich method (DR) method was also used to estimate the specific surface area (Table 6). The specific surface area of the powder clays determined by Dubinin-Radushkevich method was as follows: bentonite (197 m^2/g) > the bleaching earth, sepiolite (141 m^2/g) > attapulgite (117 m^2/g). For extrudates, the specific surface area was the same or slightly lower caused by the mechanical force during the extrusion [12–15,22–24,70–72]. In the area of 2–15 nm, a significantly higher mesopore volume was observed for bentonite compared to others clays (Fig. 3). Generally, for the powder clays, the ratio of the mesopore-to-micropore volume (V_m/V_μ) was 4–7, the lowest for bentonite and the highest for the bleaching earth (Table 6). After extrusion, V_m/V_μ ratio increased ca. 2-fold for attapulgite and sepiolite, while for bentonite and the bleaching earth it remained the same. This could be attributed to morphology of clays differing mainly in the length and thickness of the elongated particles (fibers, needle-shaped or rodlike-shaped particles, Figs. 1 and 2). In other words, materials containing long solid particles showed an increased ratio of V_m/V_μ after extrusion.

A comparison with the literature [73–76] showed a slightly higher specific surface area of 125–140 m^2/g with a similar pore volume of 0.32 cm^3/g and a 2.5-fold higher V_m/V_μ ratio for attapulgite than in the current work. On the contrary, significantly lower values of the specific surface area of 9 – 70 m^2/g and pore volume 0.04 – 0.11 cm^3/g have been reported for bentonite [50,69,77–79]. These values are typical mainly for sodium forms of bentonites. Slightly higher values of 50 – 130 m^2/g, but still lower than obtained in the current work, were reported for Ca^{2+}/Mg^{2+}-dominated bentonites (<5% Na^+) [80]. In the case of sepiolite, a wide range of the specific surface area values of 75 – 400 m^2/g has been published [52,81,82] with the value measured in the current work being somewhere in the middle of this range.

The purely mesoporous bindzil material exhibited a somewhat comparable specific surface area (157 m^2/g, [70]) and the pore volume (0.30 cm^3/g, [70]) with clay materials (Table 6).

Table 7 shows the measured contact angles for the clay materials and methylcellulose. Contact angle measurements for the clays and their interpretation in general are challenging as the measurements could be affected by temperature, water content, presence of methylcellulose, particle size, surface roughness and heterogeneity as well as pretreatment. In the current case as the samples showed absorption of the liquid, the equilibrium contact angles could not be determined. The reported

Table 4
Elemental analysis of clay materials.

No.	Sample	SiO_2/Al_2O_3 *mol/mol*	Si/Al *wt/wt*	Si *wt %*	Al *wt %*	Mg *wt %*	Others *wt%*
1	Bentonite	9	4	29	7	1	K (1), Fe (2)
2	Bleaching earth	11	5	26	5	1	K (1), Fe (2), Ca (1), S (1), Ba (0.5)
3	Attapulgite	9	5	22	5	6	K (0.5), Fe (2), Ca (1), P (0.2)
4	Sepiolite	31	16	21	1	11	K (0.5)
5	Bindzil	408	208	37	0.2	–	Na (0.6)

Table 3
Median, minimum (min), and maximum (max) particle size in nm determined by SEM. Legend: L – length, W – width.

No.	Sample	particle		fiber/needle-shape			
		median	*min-max*	*LxW*	*L/W*	*min-max (L)*	*min-max (W)*
1	Bentonite	450	30–28,000	–	–	–	–
2	Bleaching earth	195	50–850	–	–	–	–
3	Attapulgite	1000 (110)	360–8000 (70–190)	170 × 20	9	50–600	13–30
4	Sepiolite	–	–	740 × 30	25	190–3100	15–60
5	Bindzil	50	10–280	–	–	–	–

Table 5
Brønsted and Lewis acid sites of clay materials. Legend: BAS – Brønsted acid sites, LAS – Lewis acid sites, TAS – total acid sites, BAS/LAS – ratio of the Brønsted and Lewis acid sites, s (strong acid sites, data at 450 °C), m (medium acid sites, data at 350 °C minus data at 450 °C), and w (weak acid sites, data at 250 °C minus data at 350 °C).

No.	Sample	BAS				LAS				TAS	BAS/LAS
		w	*m*	*s*	∑	*w*	*m*	*s*	∑	μmol/g	-
1	Bentonite	16	20	0	36	14	5	0	19	54	2
2	Bleaching earth	46	0	0	46	8	0	0	8	54	6
3	Attapulgite	1	5	0	6	27	8	0	34	40	0.2
4	Sepiolite	6	2	0	8	55	11	0	66	73	0.1
5	Bindzil[23]	0	0	1	1	1	0	0	1	2	1

Table 6
Textural properties of powder clay and extrudates. A – specific surface area (BET: Brunauer-Emmett-Teller, DR: Dubinin-Radushkevich), V – pore volume (m: meso, μ: micro).

No.	Sample	Powder				Extrudates			
		A_{BET} m^2/g	A_{DR} m^2/g	V cm^3/g	V_m/V_μ -	A_{BET} m^2/g	A_{DR} m^2/g	V cm^3/g	V_m/V_μ -
1	Bentonite	172	197	0.25	4	152	180	0.23	4
2	Bleaching earth	120	141	0.35	7	118	142	0.35	8
3	Attapulgite	103	117	0.25	6	97	116	0.37	12
4	Sepiolite	135	141	0.31	5	106	123	0.43	11
5	Bindzil[70]	157	–	0.30	29	–	–	–	–

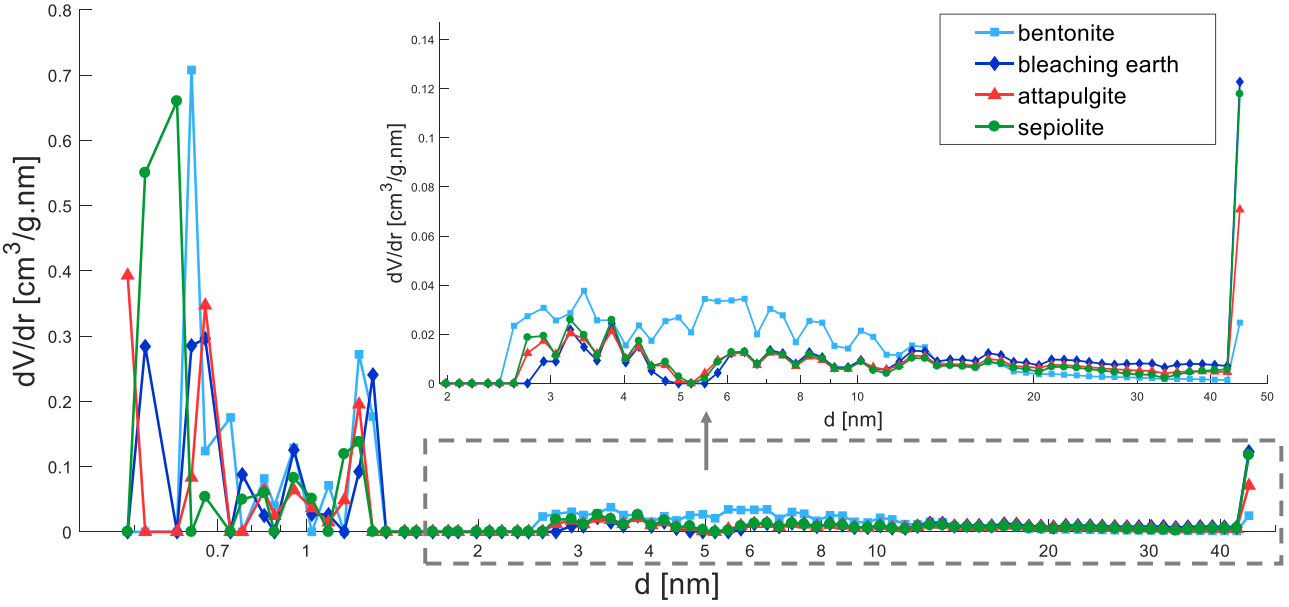

Fig. 3. Pore size distribution of clay materials.

Table 7
Contact angle (CA) of methylcellulose, bentonite, and clay material with 1 wt% of methylcellulose.

No.	Sample	CA °
	Methylcellulose (MC)	75 ± 3
	Bentonite (pristine)	19 ± 3
1	Bentonite + 1 wt% MC	23 ± 5
2	Bleaching earth + 1 wt% MC	26 ± 2
3	Attapulgite + 1 wt% MC	24 ± 3
4	Sepiolite + 1 wt% MC	23 ± 3
5	Bindzil (pristine)	17 ± 2

contact angles were, therefore, read from a specific time point in the beginning, when the droplets were somewhat stabilized while only little absorption had occurred. The contact angle was very much the same (ca. 24°) for different clay materials containing 1 wt% of methylcellulose (Table 7), thus it can be concluded that hydrophobicity is not the reason for different behavior of the clay materials during extrusion. For comparison, also contact angle of pristine bindzil, bentonite and methylcellulose were measured to be 17°, 19° and 75°, respectively.

The highest mechanical strength of extrudates of 16 MPa and 8 MPa was measured for attapulgite in both vertical and horizontal positions, respectively (Table 8). It is close to the values of commercial Al_2O_3 (BDH Ltd, Poole), namely 19.6 MPa in vertical and 7.7 MPa in the horizontal positions [15]. On the contrary, the lowest mechanical strength was obtained for sepiolite (MS (V) = 5.6 MPa, Table 8). Generally, the mechanical strength of extrudates containing a catalyst (Beta, Y, TS-1

Table 8
Mechanical strength of clay extrudates. Legend: MS (V) – average mechanical strength of 10 extrudates in vertical position, MS (H) – average mechanical strength of 10 extrudates in horizontal position.

No.	Sample	MS (V) *MPa*	MS (H)
1	Bentonite	11.5 ± 1.1	3.5 ± 0.4
2	Bleaching earth	13.8 ± 1.4	5.4 ± 0.5
3	Attapulgite	16.3 ± 1.6	7.7 ± 0.8
4	Sepiolite	5.6 ± 0.6	3.5 ± 0.4

zeolites, ZSM-5, MCM-41) and 30 wt% of inorganic binder, e.g. clay material, is ca. 0.2–4.8 MPa in a vertical position [13,15,20,83,84]. The plausible explanations for the highest mechanical strength of attapulgite in both horizontal and vertical positions can be attributed to the crystal structure, crystallinity and the crystal size of the attapulgite clay materials. This material exhibited also the highest median particle size 1000 (110) (Table 3) among four studied clay materials.

The MAS NMR spectra on ^{27}Al are shown on Fig. 4. All the materials contained peaks at 60–70 ppm and at 5–10 ppm, thus proving that the tetrahedral Al atoms are framework substitutions in Si tetrahedral layers. The signal near to 0 ppm, i.e. 5–10 ppm, is attributed to the octahedral layers. For the samples of attapulgite and bentonite the signals at 5 ppm are predominant, showing higher content of the octahedral layers. For sepiolite the amount of the tetrahedral layers (signal at 65 ppm) is higher than that of the octahedral layers (signals at 5 ppm), and the overall signal intensity is low. The relative amount of the octahedral layers was the highest for the attapulgite clay.

3.2. Catalytic results

Although the structure, chemical composition, textural properties, and especially acidity of the clays are different, the reaction rate and conversion of citronellal were comparable for all clay extrudates after 2 h of time-on-stream (TOS) (Fig. 5a,b). The initial reaction rate was the highest, $10.3 \cdot 10^{-7}$ mol.g^{-1}.s^{-1}, for bentonite and the lowest for bleaching earth, $7.5 \cdot 10^{-7}$ mol.g^{-1}.s^{-1}. The liquid phase mass balance closure (MB) increased to 85% with decreasing conversion of citronellal to 44% in 3 h of TOS for bentonite (Fig. 5b,c). This is in line with the dynamic behavior of a trickle-bed reactor under the transient state reported previously in literature [11,13,15,22,23]. The total yield of all products varied in the range of 19–26% at 2 h of TOS (Fig. 5d).

In all cases of clay extrudates, the main product were the desired isopulegol isomers (Figs. 6 and 7).

The best results were obtained over attapulgite with isopulegols yield of 24% and stereoselectivity to the isopulegol isomer of 61% (Fig. 7). No undesired products were detected, over this catalyst, although attapulgite contained a high amount of impurities (Table 4).

The highest yield and stereoselectivity to the desired products could be explained by the highest meso-to-micropore volume ratio (11.8, Table 6), the highest basicity (pH 9.9, Table 1), the low BAS/LAS ratio of 0.2, the lowest content of Brønsted acid sites (BAS 6 μmol/g, wBAS 1 μmol/g, Table 5) and the overall the lowest concentration of total acid sites (TAS 40 μmol/g, Table 5). On the contrary, the lowest yield to isopulegols of 18% with the lowest stereoselectivity to isopulegol isomer of 40%, and at the same time, the highest amount of defunctionalized products was exhibited the bleaching earth with the highest amount of Brønsted acid sites. This is in line with the literature [23] stating that

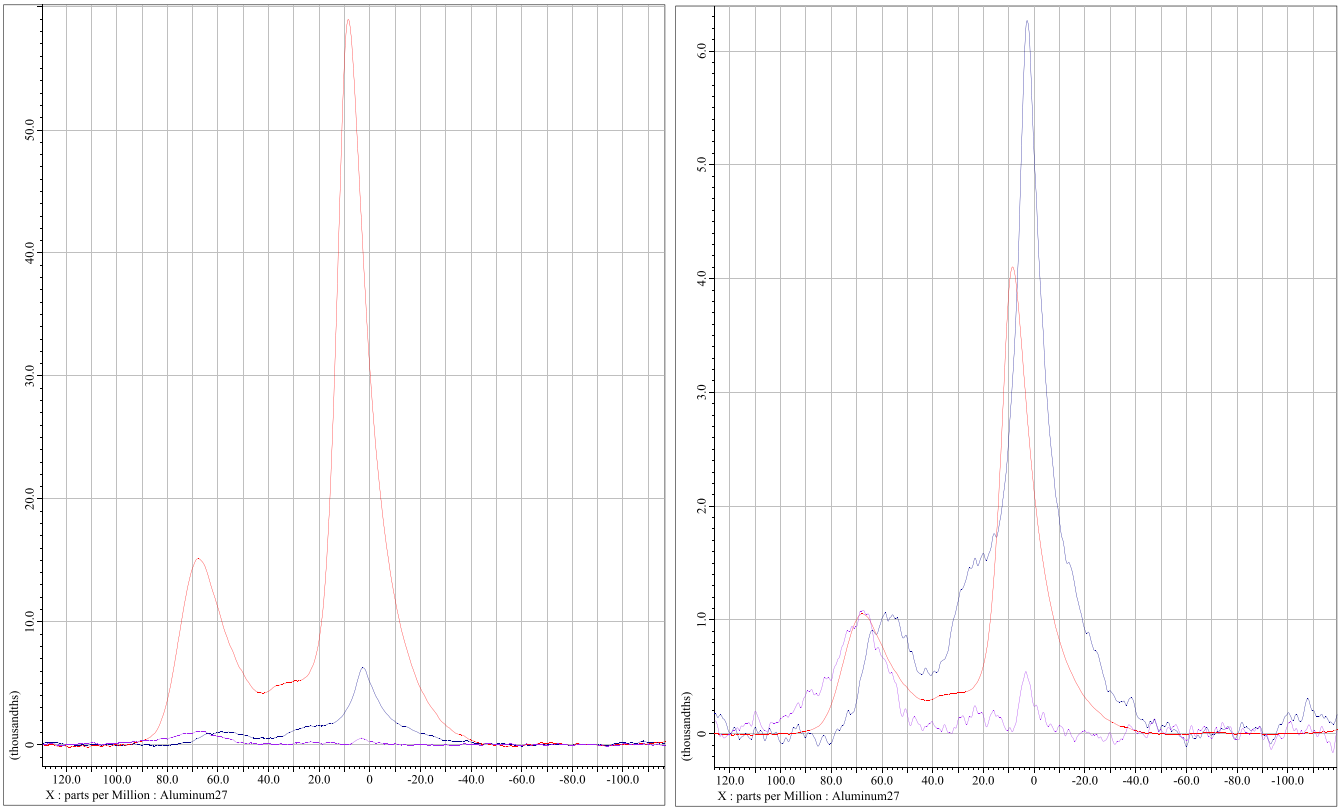

Fig. 4. ^{27}Al MAS NMR spectra of attapulgite (dark blue), bentonite (red) and sepiolite (violet) in scale (a) and normalized at 65 ppm (b).

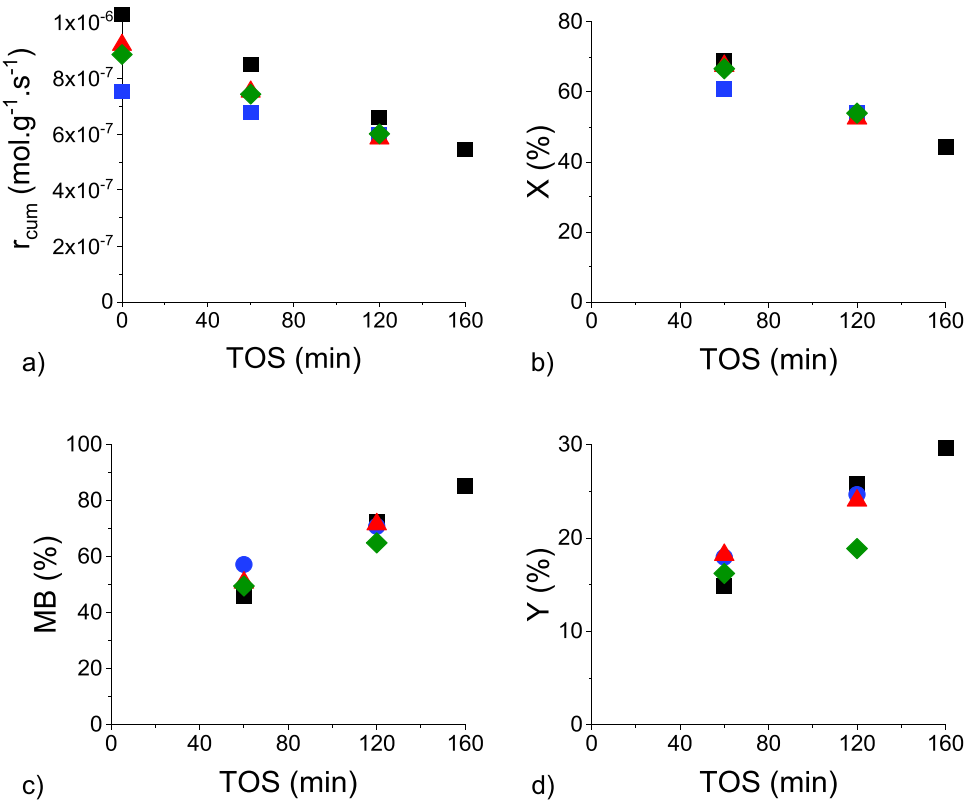

Fig. 5. Citronellal transformations over clay extrudates as a function of time-on-stream: a) cumulative reaction rate, b) citronellal conversion, c) the liquid phase mass balance closure, d) total yield. Conditions: 70 °C, 10 bar of Ar, 0.45 g of extrudates, 0.3 mL/min of citronellal in cyclohexane with initial citronellal concentration 0.086 M and 50 mL/min of Ar. Legend: bentonite (**1**, black square), bleaching earth (**2**, blue circle), attapulgite (**3**, red triangle), sepiolite (**4**, green diamond).

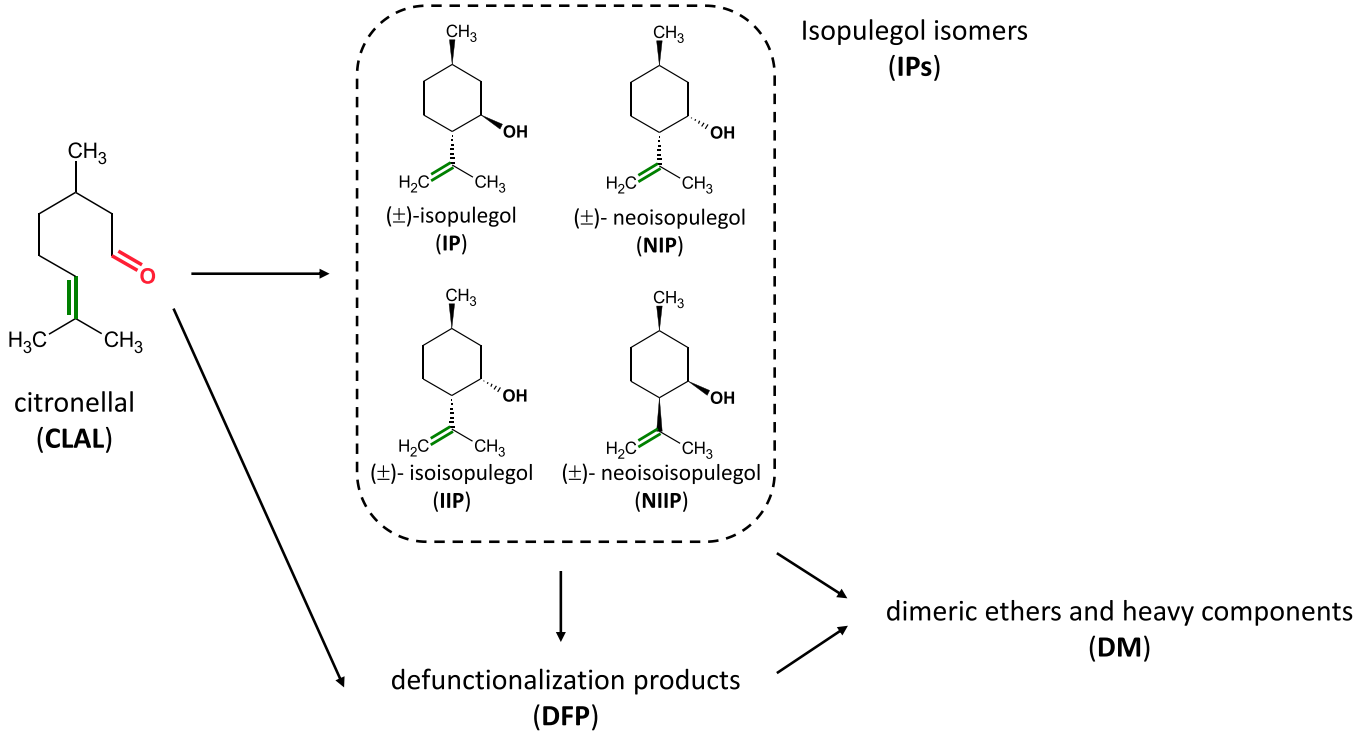

Fig. 6. Scheme of citronellal cyclization to isopulegols with potential side products over clay extrudates [22,23].

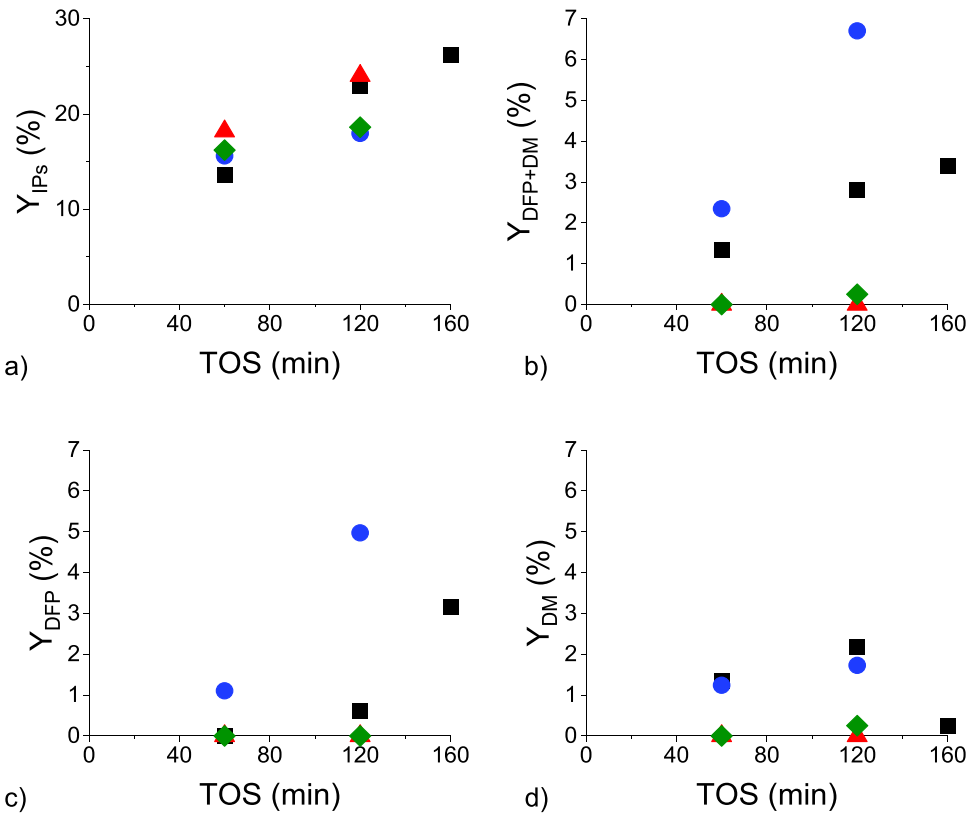

Fig. 7. Citronellal transformations over clay extrudates as a function of time-on-stream: (a) yield of isopulegols, (b) yield of undesired products, (c) yield of defunctionalization products, (d) yield of dimeric ethers and heavy components. Conditions: 70 °C, 10 bar of Ar, 0.45 g of extrudates, 0.3 mL/min of citronellal in cyclohexane with initial citronellal concentration 0.086 M and 50 mL/min of Ar. Legend: bentonite (**1**, black square), bleaching earth (**2**, blue circle), attapulgite (**3**, red triangle), sepiolite (**4**, green diamond).

Table 9
Citronellal transformations over clay extrudates at 2 h of time-on-stream. Legend: bentonite (**1**), bleaching earth (**2**), attapulgite (**3**), sepiolite (**4**), r^0 – initial reaction rate, r_{cum} – cumulative reaction time at 2 h of TOS, X – citronellal conversion, MB – the liquid phase mass balance closure, Y – total yield, SS – stereoselectivity, IPs – isopulegol isomers, DFP – defunctionalization products, DM – dimeric ethers and heavy components, IP – isopulegol, NIP – neoisopulegol, IIP – isoisopulegol, NIIP – neoisoisopulegol. Conditions: 70 °C, 10 bar of Ar, 0.45 g of extrudates, 0.3 mL/min of citronellal in cyclohexane with initial citronellal concentration 0.086 M and 50 mL/min of Ar; β-25 – data obtained in [15].

No.	r^0 $mol.g^{-1}.s^{-1}$	r_{cum}	X %	MB	Y	Y_{IPs}	Y_{DFP}	Y_{DM}	SS_{IP}	SS_{NIP}	SS_{IIP}	SS_{NIIP}
1	$10.3•10^{-7}$	$6.6•10^{-7}$	53	72	26	23	1	2	46	32	5	0
2	$7.5•10^{-7}$	$6.0•10^{-7}$	54	71	25	18	5	2	40	26	4	0
3	$9.2•10^{-7}$	$5.8•10^{-7}$	52	72	24	24	0	0	61	29	3	0
4	$8.8•10^{-7}$	$6.0•10^{-7}$	54	65	19	19	0	0	52	34	4	0
β-25	$4.9•10^{-7}$	$4.8•10^{-7}$	92	92	84	74	1	9	68	25	5	1

side products are associated with specific sites. In particular, it has been observed that cyclization to isopulegols is favored by Lewis acid sites with a low ratio of Brønsted-to-Lewis acid sites, while presence of the Brønsted acid sites, and mass transfer limitations are favorable for the side reactions [23]. Interestingly the general considerations could not be applied to sepiolite containing the highest amount of Lewis acid sites with the lowest BAS/LAS ratio (Table 5), which could be explained by a high concentration of Mg (11 wt%) and a high silica to alumina molar ratio of 31 (Table 4).

The dimeric ethers and heavy components (DM) was observed for bentonite and bleaching earth with the high amount of weak Brønsted acid sites and high BAS/LAS ratio (wBAS 16–46 μmol/g, BAS/LAS 2–6, Table 5) and different surface morphology compared to attapulgite and sepiolite, i.e. without needle-shaped nor rodlike-shaped particles.

Table 9 shows the results obtained at 2 h of TOS over clay extrudates (current work) and acidic H-β-25 extrudates without a binder [15]. It should be noted that H-β-25 is a highly acidic zeolite without impurities and with a high value of the specific surface area of 690 m^2/g, i.e. exhibiting ca. 4–7 fold higher acidity and ca. 5–7 higher specific surface area compared to the clay extrudates. This zeolite has been often investigated in cyclization of citronellal mainly in the batch mode [13, 15,35,39]. A study, somewhat comparable with the current work, was performed on citronellal cyclization over H-β-25 extrudates in the trickle-bed reactor with the same experimental setup as in herein, namely at 70 °C, 10 bar of Ar, and the same initial citronellal concentration of 0.086 M in cyclohexane. The experiments were different only in the amount of the catalyst, and the liquid residence time (1 g of catalyst, RT 12.5 min for H-β-25 [15]; 0.45 g of catalyst, RT 5.3 min for clays). In the case of H-β-25 zeolite, a comparison clearly shows high yield to isopulegols of 74% with the highest stereoselectivity to the desired isopulegol isomer of 68% and also the higher amount of the dimeric ethers and heavy components. Contrary to the expectations, the initial reaction rate was ca. 2-fold higher for bentonite.

At the same time, for attapulgite, the stereoselectivity to the desired isopulegol isomer as an intermediate for (-)-menthol isomer having a strong physiological cooling effect [85,86] was similar with H-β-25 zeolite (namely 61 vs 68%, Table 9). In other cases, stereoselectivity to isopulegol was lower, especially for bleaching earth (40%) and bentonite (46%, Table 9). Overall, the stereoselectivity of isopulegol/neoisopulegol/isoisopulegol/neoisopulegol was only slightly

lower for attapulgite (61/29/4/0) compared to the H-β-25 zeolite (68/25/5/1) (Table 9). In addition, no neoisoisopulegol was observed for clays. The effect of clay structure on stereoselectivity has not been directly demonstrated.

4. Conclusions

Four different powder clay materials were shaped into cylindrical bodies by extrusion. The diameter of the final extrudates (1.3–1.42 mm) linearly decreased with decreasing concentration of the clay material in the optimal suspension for extrusion. Clays were characterized in depth by electron microscopes, nitrogen physisorption, pyridine Fourier transform infrared, potential of hydrogen measurement, contact angle measurements, ^{27}Al magic-angle-spinning nuclear magnetic resonance, and the crush test. For comparison, also a pristine colloidal silica bindzil without impurities was selected and characterized in the current work.

Catalytic properties of clay extrudates were investigated in citronellal cyclization as a model reaction, which was performed in a trickle-bed reactor at 70 °C, under 10 bar total pressure of argon with 0.086 M initial citronellal concentration in cyclohexane.

Results clearly showed that clays themselves are not inert and they have catalytic properties in the studied reaction. Although the structure, chemical composition, textural properties, and acidity of the extrudates were different, the reaction rate and conversion of citronellal were comparable for all clay extrudates at 2 h of time-on-stream. The best results were obtained over attapulgite with isopulegols yield of 24% and stereoselectivity to the desired isopulegol isomer of 61%. No undesired products were detected. Attapulgite had the highest meso-to-micropore volume ratio, the highest basicity, the low Brønsted-to-Lewis acid sites ratio of 0.2, and the lowest amount of Brønsted acid sites compared to bentonite, bleaching earth and sepiolite extrudates. In addition, the same clay exhibited the highest mechanical strength.

CRediT authorship contribution statement

Zuzana Vajglová: Investigation, Visualization, Writing – original draft. **Mark Martinez-Klimov**: Investigation. **Irina L. Simakova**: Investigation. **Päivi Mäki-Arvela**: Supervision, Writing – review & editing. **Narendra Kumar**: Investigation, Supervision. **Markus Peurla**: Investigation. **Alexander Efimov**: Investigation. **Leena Hupa**: Supervision. **Stiina Tolvanen**: Investigation. **Jouko Peltonen**: Supervision. **Dmitry Yu. Murzin**: Conceptualization, Writing – review & editing, Supervision, Project administration.

Declaration of Competing Interest

The authors declare that they have no known competing financial interests or personal relationships that could have appeared to influence the work reported in this paper.

Acknowledgments

The authors are grateful to Academy of Finland for funding through the project: Synthesis of spatially controlled catalysts with superior performance. Electron microscopy samples were processed and analyzed at the Electron Microscopy Laboratory, Institute of Biomedicine, University of Turku, which receives financial support from Biocenter Finland. The authors are grateful to Mark Martinez-Klimov for the pH measurements. I.S. is grateful for the support from the Ministry of Science and Higher Education of the Russian Federation, under the governmental order for Boreskov Institute of Catalysis (Project No. AAAAA21-121011390055-8).

References

[1] G.E. Christidis, Assessment of Industrial Clays, in: Handbook of Clay Science, Developments in Clay Science, 2013.
[2] H.H. Murray, Applied Clay Mineralogy: Occurrences, Processing and Applications of Kaolins, Bentonites, Palygorskite-Sepiolite, and Common Clays, Elsevier Sience, 2006.
[3] F. Dorado, R. Romero, P. Canizares, Influence of clay binders on the performance of Pd/HZSM-5 catalysts for the hydroisomerization of *n*-butane, Ind. Eng. Chem. Res. 40 (2001) 3428–3434.
[4] R.D. Holtz, W.D. Kovacs, T.C. Sheahan, An Introduction to Geotechnical Engineering, Prentice-Hall, 1981.
[5] G. Lagaly, S. Ziesmer, Colloid chemistry of clay minerals: the coagulation of montmorillonite dispersions, Adv. Colloid Interface Sci. 100 (2003) 105–128.
[6] C.H. Zhou, An overview on strategies towards clay-based designer catalysts for green and sustainable catalysis, Appl. Clay Sci. 53 (2011) 87–96.
[7] D. Gournis, L. Jankovic, E. Maccallini, D. Benne, P. Rudolf, J.F. Colomer, C. Sooambar, V. Georgakilas, M. Prato, M. Fanti, F. Zerbetto, G.H. Sarova, D. M. Guldi, Clay-fulleropyrrolidine nanocomposites, J. Am. Chem. Soc. 128 (2006) 6154–6163.
[8] V.C. Kelessidis, R. Maglione, Yield stress of water-bentonite dispersions, Colloid Surf. A-Physicochem. Eng. Asp. 318 (2008) 217–226.
[9] J.K. Mitchell, K. Soga, Fundamentals of Solid Behavior, Hoboken, N.J.: John Wiley & Sons, 2005.
[10] H. Hernando, C. Ochoa-Hernandez, M. Shamzhy, I. Moreno, J. Fermoso, P. Pizarro, J.M. Coronado, J. Cejka, D.P. Serrano, The crucial role of clay binders in the performance of ZSM-5 based materials for biomass catalytic pyrolysis, Catal. Sci. Technol. 9 (2019) 789–802.
[11] M. Azkaar, P. Mäki-Arvela, Z. Vajglová, V. Fedorov, N. Kumar, L. Hupa, J. Hemming, M. Peurla, A. Aho, D. Yu, Murzin, synthesis of menthol from citronellal over supported Ru- and Pt-catalysts in continuous flow, React. Chem. Eng. 4 (2019) 2156–2169.
[12] Z. Vajglová, N. Kumar, M. Peurla, J. Peltonen, I. Heinmaa, D. Yu, Murzin, synthesis and physicochemical characterization of beta zeolite-bentonite composite materials for shaped catalysts, Catal. Sci. Technol. 8 (2018) 6150–6162.
[13] Z. Vajglová, N. Kumar, P. Mäki-Arvela, K. Eränen, M. Peurla, L. Hupa, D. Yu, Murzin, effect of binders on the physicochemical and catalytic properties of extrudate-shaped beta zeolite catalysts for cyclization of citronellal, Org. Process. Res. Dev. 23 (2019) 2456–2463.
[14] Z. Vajglová, N. Kumar, M. Peurla, L. Hupa, K. Semikin, D.A. Sladkoyskiy, D. Yu, Murzin, effect of the preparation of Pt-modified zeolite beta-bentonite extrudates on their catalytic behavior in *n*-hexane hydroisomerization, Ind. Eng. Chem. Res. 58 (2019) 10875–10885.
[15] Z. Vajglová, N. Kumar, P. Mäki-Arvela, K. Eränen, M. Peurla, L. Hupa, M. Nurmi, M. Toivakka, D. Yu, Murzin, synthesis and physicochemical characterization of shaped catalysts of beta and Y zeolites for cyclization of citronellal, Ind. Eng. Chem. Res. 58 (2019) 18084–18096.
[16] V.K. Saini, M. Pinto, J. Pires, Natural clay binder based extrudates of mesoporous materials: improved materials for selective adsorption of natural and biogas components, Green. Chem. 13 (2011) 1251–1259.
[17] S. Bueno, E. Duran, B. Gamiz, M.C. Hermosin, Formulating low cost modified bentonite with natural binders to remove pesticides in a pilot water filter system, J. Environ. Chem. Eng. 9 (2021), 104623.
[18] R.W. Grimshaw, The Chemistry and Physics of Clays, Wiley-Interscience, 1971.
[19] S. He, I. Muizebelt, A. Heeres, N.J. Schenk, R. Blees, H.J. Heeres, Catalytic pyrolysis of crude glycerol over shaped ZSM-5/bentonite catalysts for bio-BTX synthesis, Appl. Catal. B 235 (2018) 45–55.
[20] D.P. Serrano, R. Sanz, P. Pizarro, I. Moreno, P. de Frutos, S. Blazquez, Preparation of extruded catalysts based on TS-1 zeolite for their application in propylene epoxidation, Catal. Today 143 (2009) 151–157.
[21] R.V. Jasra, B. Tyagi, Y.M. Badheka, V.N. Choudary, T.S.G. Bhat, Effect of clay binder on sorption and catalytic properties of zeolite pellets, Ind. Eng. Chem. Res. 42 (2003) 3263–3272.
[22] Z. Vajglová, N. Kumar, M. Peurla, K. Eränen, P. Mäki-Arvela, D. Yu, Murzin, cascade transformations of (±)-citronellal to Menthol over extruded Ru-MCM-41 catalysts in a continuous reactor, Catal. Sci. Technol. 10 (2020) 8108–8119.
[23] Z. Vajglová, P. Mäki-Arvela, K. Eränen, N. Kumar, M. Peurla, D. Yu, Murzin, catalytic transformations of citral in a continuous flow over bifunctional Ru-MCM-41 extrudates, Catal. Sci. Technol. 11 (2021) 2873–2884.
[24] Z. Vajglová, N. Kumar, M. Peurla, L. Hupa, K. Semikin, D.A. Sladkovskiy, D. Y. Murzin, Deactivation and Regeneration of Pt-modified Zeolite Beta–Bindzil Extrudates in *n*-Hexane Hydroisomerization, J. Chem. Technol. Biotechnol. 96 (2021) 1645–1655.
[25] G.T. Whiting, F. Meirer, M.M. Mertens, A.J. Bons, B.M. Weiss, P.A. Stevens, E. de Smit, B.M. Weckhuysen, Binder effects in SiO_2- and Al_2O_3-bound zeolite ZSM-5-based extrudates as studied by microspectroscopy, ChemCatChem 7 (2015) 1312–1321.
[26] J. Zecevic, G. Vanbutsele, K.P. de Jong, J.A. Martens, Nanoscale intimacy in bifunctional catalysts for selective conversion of hydrocarbons, Nature 528 (2015) 245–248.
[27] F. Dorado, R. Romero, P. Canizares, Hydroisomerization of *n*-butane over Pd/HZSM-5 and Pd/H beta with and without binder, Appl. Catal. A-Gen. 236 (2002) 235–243.
[28] H. Liu, Y.M. Zhou, Y.W. Zhang, L.Y. Bai, M.H. Tang, Influence of binder on the catalytic performance of PtSnNa/ZSM-5 catalyst, for propane dehydrogenation, Ind. Eng. Chem. Res. 47 (2008) 8142–8147.

[29] J.S.J. Hargreaves, A.L. Munnoch, A survey of the influence of binders in zeolite catalysis, Catal. Sci. Technol. 3 (2013) 1165–1171.
[30] S. Mitchell, N.L. Michels, J. Perez-Ramirez, From powder to technical body: the undervalued science of catalyst scale up, Chem. Soc. Rev. 42 (2013) 6094–6112.
[31] W.J. Roth, J. Cejka, Two-dimensional zeolites: dream or reality? Catal. Sci. Technol. 1 (2011) 43–53.
[32] N.Y. Chen, M.C. Liu, S.C. Yang, H.S. Sheu, J.R. Chang, Impacts of binder-zeolite interactions on the structure and surface properties of NaY-SiO_2 extrudates, Ind. Eng. Chem. Res. 54 (2015) 8456–8468.
[33] P. Mäki-Arvela, L.P. Tiainen, A.K. Neyestanaki, R. Sjöholm, T.K. Rantakyla, E. Laine, T. Salmi, D. Yu, Murzin, liquid phase hydrogenation of citral: suppression of side reactions, Appl. Catal. A-Gen. 237 (2002) 181–200.
[34] P. Mäki-Arvela, L.P. Tiainen, M. Lindblad, K. Demirkan, N. Kumar, R. Sjöholm, T. Ollonqvist, J. Vayrynen, T. Salmi, D. Yu, Murzin, liquid-phase hydrogenation of citral for production of citronellol: catalyst selection, Appl. Catal. A-Gen. 241 (2003) 271–288.
[35] P. Mäki-Arvela, N. Kumar, V. Nieminen, R. Sjöholm, T. Salmi, D. Yu, Murzin, cyclization of citronellal over zeolites and mesoporous materials for production of isopulegol, J. Catal. 225 (2004) 155–169.
[36] P. Mäki-Arvela, N. Kumar, D. Kubička, A. Nasir, T. Heikkilä, V.P. Lehto, R. Sjöholm, T. Salmi, D. Yu, Murzin, one-pot citral transformation to menthol over bifunctional micro- and mesoporous metal modified catalysts: effect of catalyst support and metal, J. Mol. Catal. A-Chem. 240 (2005) 72–81.
[37] I. Fatimah, D. Rubiyanto, T. Huda, Effect of sulfation on zirconia-pillared montmorillonite to the catalytic activity in microwave-assisted citronellal conversion, Int. J. Chem. React. Eng. 950190 (2014), 7-7.
[38] A.B. Dongil, L. Pastor-Perez, J.L.G. Fierro, N. Escalona, A. Sepulveda-Escribano, Effect of the surface oxidation of carbon nanotubes on the selective cyclization of citronellal, Appl. Catal. A-Gen. 524 (2016) 25–31.
[39] M. Vandichel, F. Vermoortele, S. Cottenie, D.E. De Vos, M. Waroquier, V. Van, Speybroeck, insight in the activity and diastereoselectivity of various lewis acid catalysts for the citronellal cyclization, J. Catal. 305 (2013) 118–129.
[40] P.R.S. Braga, A.A. Costa, E.F. de Freitas, R.O. Rocha, J.L. de Macedo, A.S. Araujo, J. A. Dias, S.C.L. Dias, Intramolecular cyclization of (+)-citronellal using supported 12-tungstophosphoric acid on MCM-41, J. Mol. Catal. A-Chem. 358 (2012) 99–105.
[41] A.K. Shah, S. Park, H.A. Khan, U.H. Bhatti, P. Kumar, A.W. Bhutto, Y.H. Park, Citronellal cyclisation over heteropoly acid supported on modified montmorillonite catalyst: effects of acidity and pore structure on catalytic activity, Res. Chem. Intermed. 44 (2018) 2405–2423.
[42] P. Muller, P. Wolf, I. Hermans, Insights into the complexity of heterogeneous liquid-phase catalysis: case study on the cyclization of citronellal, ACS Catal. 6 (2016) 2760–2769.
[43] C. Jimeno, J. Miras, J. Esquena, $TiO_2(SiO_2)(x)$ and $ZrO_2(SiO_2)(x)$ cryogels as catalysts for the citronellal cyclization to isopulegol, Catal. Lett. 143 (2013) 616–623 [43] F. Neatu, S. Coman, V. I. Parvulescu, G. Poncelet, D. de Vos, P. Jacobs, Heterogeneous Catalytic Transformation of Citronellal to Menthol in a Single Step on Ir-Beta Zeolite Catalysts, Top. Catal., 2009, 52, 1292–1300.
[44] E. Vrbková, T. Prejya, M. Lhotka, E. Vzskočilová, L. Červený, Fe-modified zeolite BETA as an active catalyst for intramolecular prins cyclization of citronellal, Catal. Lett. 151 (2021) 1993–2003.
[46] V. Kuuluvainen, P. Mäki-Arvela, A.R. Rautio, K. Kordas, J. Roine, A. Aho, B. Toukoniitty, H. Österholm, M. Toivakka, D. Yu, Murzin, properties of adsorbents used for bleaching of vegetable oils and animal fats, J. Chem. Technol. Biotechnol. 90 (2015) 1579–1591.
[47] V. Kuuluvainen, P. Mäki-Arvela, K. Eränen, A. Holappa, J. Hemming, H. Österholm, B. Toukoniitty, D. Yu, Murzin, extraction of spent bleaching earthin the production of renewable diesel, Chem. Eng. Technol. 38 (2015) 769–776.
[48] A. Azzolini, V.M. Sglavo, J.A. Downs, Novel method for the identification of the maximum solid loading suitable for optimal extrusion of ceramic pastes, J. Adv. Ceram. 3 (2014) 7–16.
[49] ImageJ program, ⟨https://imagej.net/Welcome⟩ (accessed October 2021).
[50] C.A. Emeis, Determination of integrated molar extinction coefficients for infrared-adsorption bands of pyridine adsorbed on solid acid catalysts, J. Catal. 141 (1993) 347–354.
[51] D.Yu. Murzin, Engineering Catalysis, Walter de Gruyter, Gottingen, 2013.
[52] Q.G. Tang, F. Wang, M.R. Tang, J.S. Liang, C.Y. Ren, Study on pore distribution and formation rule of sepiolite mineral nanomaterials, J. Nanomater. 2012 (2012) 1–6.
[53] B.M. Das, Advanced Soil Mechanics, CRC Press, 2013.
[54] S. Gueu, G. Finqueneisel, T. Zimny, D. Bartier, B.K. Yao, Physicochemical characterization of three natural clays used as adsorbent for the humic acid removal from aqueous solution, Adsorp. Sci. Technol. 37 (2018) 77–94.
[55] B.K.G. Theng, Formation and properties of clay-polymer complexes, chapter 1 the clay minerals, Dev. Soil Sci. 9 (1979) 3–36.
[56] W.M. Ye, Y. He, Y.G. Chen, B. Chen, Y.J. Cui, Thermochemical effects on the smectite alteration of GMZ bentonite for deep geological repository, Environ. Earth Sci. 75 (2016) 1–11.
[57] S.L. Abdullahi, A.A. Audu, Comparative analysis on chemical composition of bentonite clays obtained from ashaka and tango deposits in Gombe State, Nigeria, ChemSearch J. 8 (2017) 35–40.
[58] B. Liu, H. Sun, T. Peng, Q. He, One-step synthesis of hydroxysodalite using natural bentonite at moderate temperatures, Minerals 8 (2018) 521.
[59] S. Oumnih, N. Bekkouch, E.K. Gharibi, N. Fagel, K. Elhamouti, M.E. Ouahabi, Phosphogypsum waste as additives to lime stabilization of bentonite, Sustain. Environ. Res. 29 (2019) 25–35.
[60] S. Srilai, W. Tanwongwan, K. Onpecth, T. Wongkitikun, K. Panpiemrasda, G. Panomsuwan, A. Eiad-ua, Synthesis of zeolite A from bentonite via hydrothermal method: the case of different base solution, AIP Conf. Proc. 2279 (2020) 0600061–0600066.
[61] W. Hamza, Ch Chtara, M. Benzina, Purification of industrial phosphoric acid (54%) using fe-pillared bentonite, Environ. Sci. Pollut. Res. 23 (2016) 15820–15831.
[62] V.S. Babaeva, A.R. Kariev, Chemical composition of paleogene bentonites of the tadzhik, Depress, Akad. Nauk Tadzhikskoi SSR 34 (1991) 439–442.
[63] Sh.A. Yusifova, S.A. Alekperova, Z.G. Zul'fugarov, Chemical composition of bentonite clays of ali-bairamly (Kazakh) and Kabystan Deposits in Azerbaidzhan S. S.R, Azerbaidzhanskii Khimicheskii Zh. 6 (1968) 79–83.
[64] D.A. Gol'dberg, S.Sh Abramovich, I.I. Cherek, Catalytic properties of bleaching clay, Khimiya i Tekhnologiya Topl. i Masel. 3 (1958) 57–60.
[65] C. Abdelouahab, H. Ait-Amar, T. Obretenov, A. Gaid, Physicochemical and structural characteristics of some bentonitic clays from North-Western Algeria, Analusis 16 (1988) 292–299.
[66] A. Ramírez, C. Sifuentes, F.S. Manciu, S. Komarneni, K.H. Pannell, R.R. Chianelli, The effect of Si/Al ratio and moisture on an organic/inorganic hybrid material: thioindigo/montmorillonite, Appl. Clay Sci. 51 (2011) 61–67.
[67] A.S. Ahmed, N. Salahudeen, C.S. Ajinomoh, H. Hamza, A. Ohikere, Studies on the mineral and chemical characteristics of pindiga bentonitic clay, Petrol. Tech. Dev. J. 1 (2012) 1–8.
[68] G.M. do Nascimento, Clay, Clay Minerals and Ceramic Materials Based on Clay Minerals, InTech, Croatia, 2016.
[69] F.M.T. Luna, J.A. Cecilia, R.M.A. Saboya, D. Barrera, K. Sapag, E. Rodriguez-Castellon, C.L. Cavalcante, Natural and Modified Montmorillonite Clays as Catalysts for Synthesis of Biolubricants, Materials 11 (2018) 1764.
[70] V.V. Zhivonitko, Z. Vajglová, P. Mäki-Arvela, N. Kumar, M. Peurla, D. Yu, Murzin, diffusion measurements of hydrocarbons in zeolite with pulse-field gradient nuclear magnetic resonance spectroscopy, Russ. J. Appl. Chem. 95 (2021) 547–557.
[71] A. de Lucas, P. Sanchez, A. Funez, M.J. Ramos, J.L. Valverde, Liquid-phase hydroisomerization of *n*-octane over platinum-containing zeolite-based catalysts with and without binder, Ind. Eng. Chem. Res. 45 (2006) 8852–8859.
[72] A. Aranzabal, D. Iturbe, M. Romero-Saez, M.P. Gonzalez-Marcos, J.R. Gonzalez-Velasco, J.A. Gonzalez-Marcos, Optimization of process parameters on the extrusion of honeycomb shaped monolith of H-ZSM-5 zeolite, Chem. Eng. J. 162 (2010) 415–423.
[73] A. Mahandrimanana, Analysis of specific surfaces of composite material: clays of madagascar and TiO_2, J. Mater. Chem. 10 (2020) 1–4.
[74] L. Boudriche, R. Calvet, B. Hamdi, H. Balard, Surface properties evolution of attapulgite by IGC analysis as a function of thermal treatment, Colloid Surf. A-Physicochem. Eng. Asp. 399 (2012) 1–10.
[75] L. Boudriche, A. Chamayou, R. Calvet, B. Hamdi, H. Balard, Influence of different dry milling processes on the properties of an attapulgite clay, contribution of inverse gas chromatography, Powder Technol. 254 (2014) 352–363.
[76] S.M. Tichapondwa, J.B. van Bijon, Adsorption of Cr (VI) pollutants in water using natural and modified attapulgite clay, Chem. Eng. Trans. 74 (2019) 355–360.
[77] K. Al-Essa, Activation of Jordanian Bentonite by Hydrochloric Acid and Its Potential for Olive Mill Wastewater Enhanced Treatment, *J. Chem.*, 2018: **2018**.
[78] M. Vlasova, G. Dominguez-Patino, N. Kakazey, M. Dominguez-Patino, D. Juarez-Romero, Y.E. Mendez, Structural-phase transformations in bentonite after acid treatment, Sci. Sinter. 35 (2003) 155–166.
[79] B. Hamdi, Z. Kessaissia, J.B. Donnet, T.K. Wang, IGC characterization of surface energy and morphology of two natural fillers: kieselguhr and bentonite, ACSM 25 (2000) 481–494.
[80] S. Kaufhold, R. Dohrmann, M. Klinkenberg, S. Siegesmund, K. Ufer, N_2-BET specific surface area of bentonites, J. Colloid Interface Sci. 349 (2010) 275–282.
[81] M. Suarez, E. Garcia-Romero, Variability of the surface properties of sepiolite, Appl. Clay Sci. 67–68 (2012) 72–82.
[82] S. Inagaki, Y. Fukushima, H. Doi, O. Kamigaito, Pore-size distribution and adsorption selectivity of sepiolite, Clay Miner. 25 (1990) 99–105.
[83] J. Lefevere, L. Protasova, S. Mullens, V. Meynena, 3D-printing of hierarchical porous ZSM-5: the importance of the binder system, Mater. Des. 134 (2017) 331–341.
[84] K.Y. Lee, H.K. Lee, S.K. Ihm, Influence of catalyst binders on the acidity and catalytic performance of HZSM-5 zeolites for methanol-to-propylene (MTP) process: single and binary binder system, Top. Catal. 53 (2010) 247–253.
[85] A. Zuliani, C.M. Cova, R. Manno, V. Sebastian, A.A. Romero, R. Luque, Continuous flow synthesis of menthol via tandem cyclisation-hydrogenation of citronellal catalysed by scrap catalytic converters, Green. Chem. 22 (2020) 379–387.
[86] J. Plösser, M. Lucas, J. Wärnå, T. Salmi, D.Y. Murzin, P. Claus, Kinetics of the one-pot transformation of citronellal to menthols on Ru/H-BEA catalysts, Org. Process. Res. Dev. 20 (2016) 1647–1653.